

Research Article

Uranium Dust Cloud Combustion: Burning Characteristics and Absorption Spectroscopy Measurements

Emily N. Weerakkody ^{1,2}, Brian A. Read,^{3,4} Michael D. Clemenson,⁵
and Nick G. Glumac ²

¹*Energetic Materials Center, Lawrence Livermore National Laboratory, Livermore, CA 94550, USA*

²*Mechanical Science and Engineering Department, University of Illinois at Urbana-Champaign, Urbana, IL 61801, USA*

³*Fleet Readiness Center East, Naval Air Systems Command, Cherry Point, NC 28532, USA*

⁴*Aerospace Engineering Department, University of Illinois at Urbana-Champaign, Urbana, IL 61801, USA*

⁵*Sandia National Laboratories, Albuquerque, NM 87123, USA*

Correspondence should be addressed to Emily N. Weerakkody; weerakkody1@llnl.gov

Received 21 September 2022; Revised 1 November 2022; Accepted 3 November 2022; Published 16 November 2022

Academic Editor: Benjamin Shaw

Copyright © 2022 Emily N. Weerakkody et al. This is an open access article distributed under the Creative Commons Attribution License, which permits unrestricted use, distribution, and reproduction in any medium, provided the original work is properly cited.

This study characterized uranium metal dust cloud combustion using absorption spectroscopy, imaging, and broadband emission measurements. Other metals were similarly combusted to establish correlations between results from this study and those found in the literature. It was determined that the burn temperature of uranium was limited to the volatilization temperature of uranium dioxide. Combustion behavior was similar to that of other refractory metals in terms of burn time and the observation of exploding particle behavior.

1. Introduction

Uranium metal is used in a variety of applications in which combustion can occur, either as a desired effect or as a potential hazard. For example, combustion of metal from armor-piercing, depleted uranium projectiles can cause significant damage [1]. In general, limited work has been published on the combustion of uranium [2–6].

Due to its pyrophoric nature, uranium powder exposed to air at room temperature forms an oxide layer primarily comprising UO_2 [4, 7–9]. Calculations performed using NASA CEA [10] with constant enthalpy and pressure (and $\varphi=1$) indicate that the adiabatic flame temperature of uranium in air and oxygen are 3773 K and 4843 K, respectively. Actual flame temperatures of clouds of uranium particles will likely vary spatially and temporally and may be significantly lower in general.

Mouradian and Baker Jr. created a model for determining uranium and zirconium burning temperatures in air with respect to sample size, geometry, and airflow whilst

making some allowance for the oxide layer [3]. From this work, for a spherical particle under natural convection and a size of less than 0.01 cm and decreasing, the burning temperature approaches about 3200 K. Due to the high boiling point of uranium (~4400 K) as compared to its oxide (~3800 K) and burning temperature at atmospheric pressure, it is expected to burn heterogeneously limited by the amount of oxide [11–13]. As in the case of Zr and Ti combustion, the suboxide UO is also expected to form a range of liquid solutions with the metal [14, 15], and therefore behave similarly in combustion.

Dust explosions involve the combustion of particulate dispersed in air and require the presence of several components: fuel, oxidation, confinement, mixing, and ignition source [16]. Dust explosions have often been studied in the context of worker safety and the prevention of accidental occurrences in environments such as coal mines [17]. Thermobaric weapons also operate in this manner, wherein an aerosol or dust-like fuel is dispersed and subsequently detonated [18]. According to electrical safety standards, a

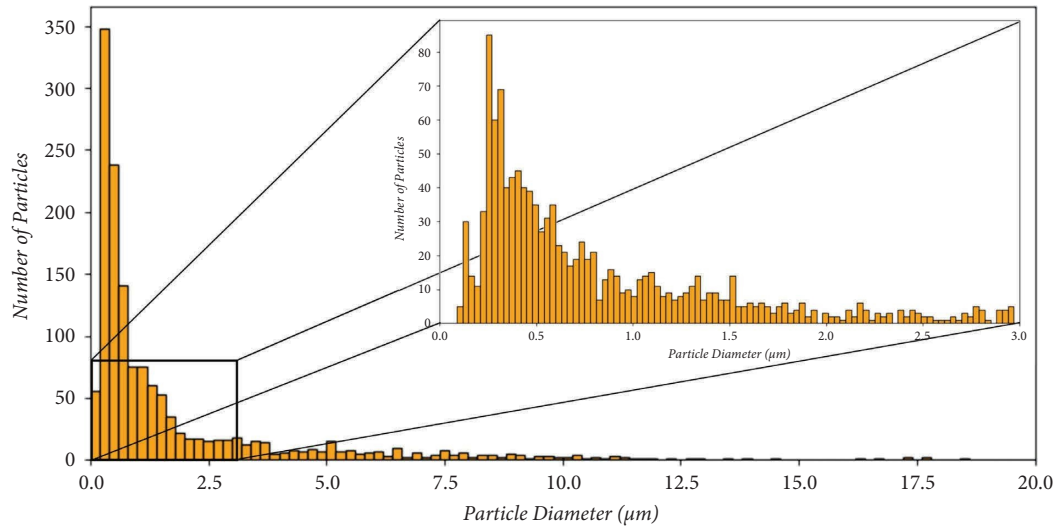


FIGURE 1: Uranium powder size distribution [38].

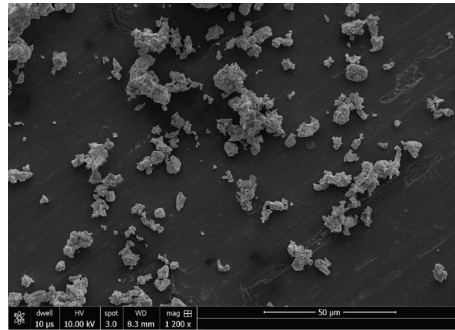


FIGURE 2: ESEM image of uranium powder particles [38].

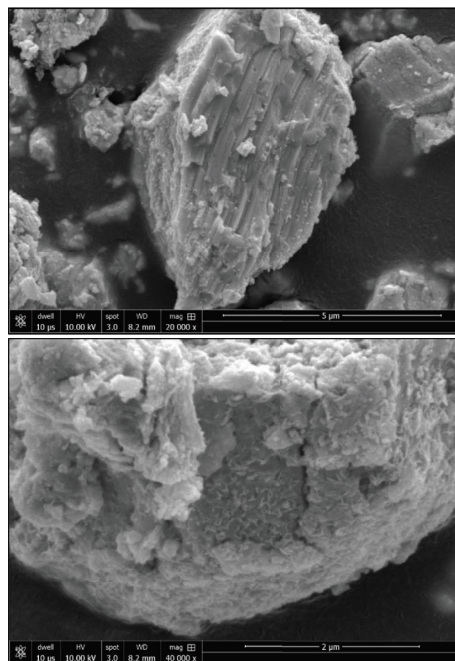


FIGURE 3: Higher resolution ESEM images of singular uranium particle. Small flecks and fuzzy irregularities on surface are likely due to uranium oxide layer [38].

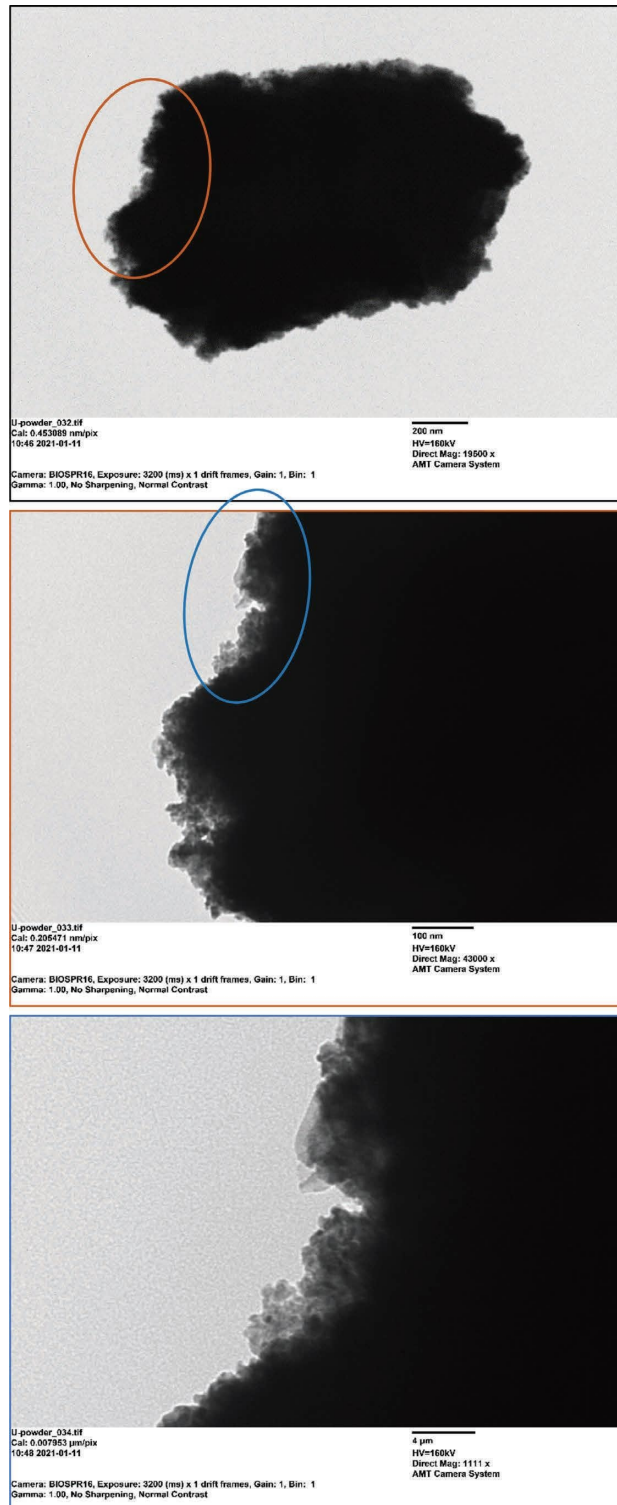


FIGURE 4: STEM images of a particle and its oxide layer at increasing magnification levels [38].

uranium dust cloud is considered potentially hazardous and electrically conductive and has a low ignition temperature [19]. A model has also previously been created to simulate aerosolized uranium dispersion in the context of potential health and safety effects [20]. These circumstances may be present when uranium is processed as fuel for nuclear reactors, and in other scenarios where uranium is combusting

[21]. Thus, dust combustion of uranium at various scales, in single particles and in variously sized clouds, is of interest.

Various experiments have been performed and models set up to study and emulate high-temperature plasma-like behavior and oxidation phenomena, which might occur in a nuclear fireball. Species that may evolve during uranium excitation, such as atomic uranium and oxides of uranium,

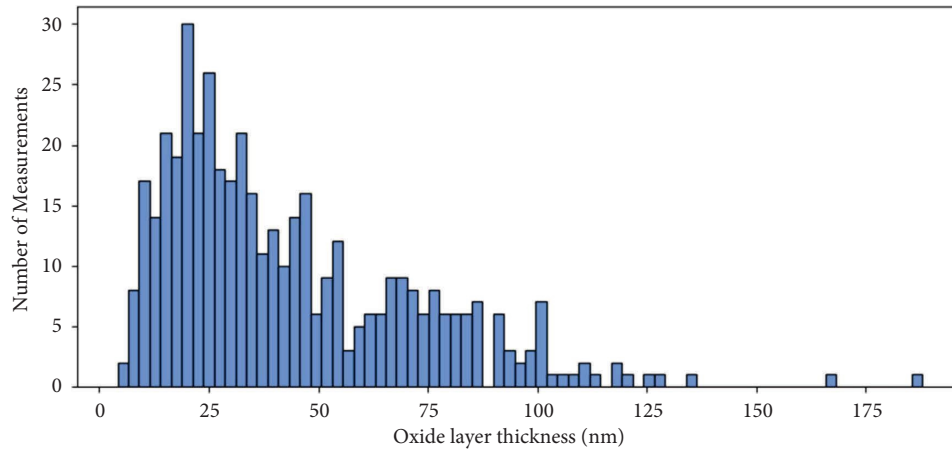


FIGURE 5: Uranium powder oxide layer thickness distribution [38].

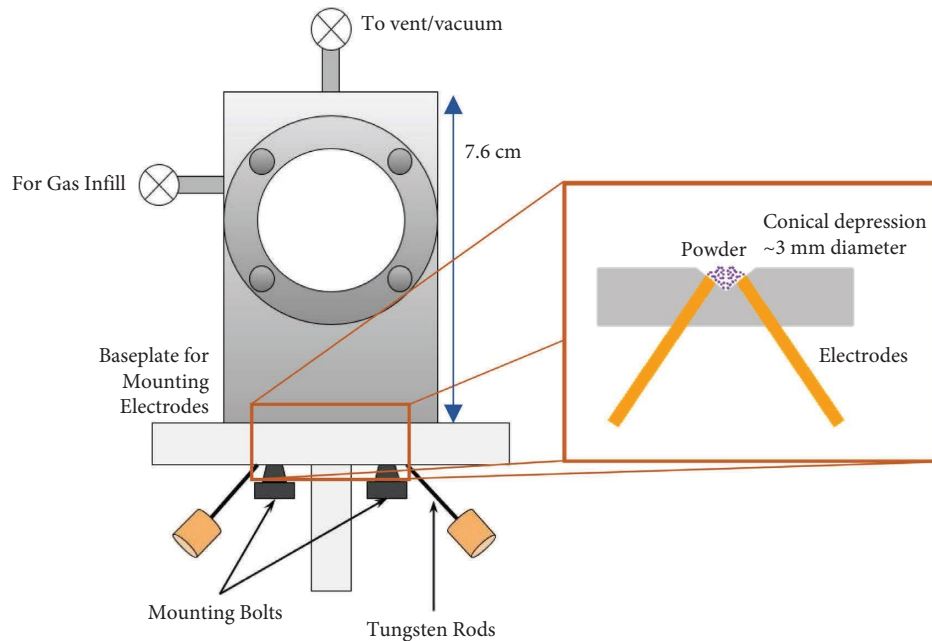


FIGURE 6: Dust cloud chamber schematic [38, 41].

have been investigated by various groups. Many uranium and uranium monoxide transitions were determined by the work of Kaledin et al., in which vapor created from the heating of uranium samples was characterized using laser-induced fluorescence (LIF) [22]. They further characterized uranium monoxide bands using pulsed laser deposition in a supersonic expansion [23]. Laser-induced breakdown spectroscopy has been used as an analog to fireball conditions to study uranium kinetics in the presence of oxygen [24–28]. A reaction mechanism has been determined and calculations performed based on these experimental results [29, 30]. Koroglu et al. observed the condensation of gas phase species into particulate from a plasma flow reactor in the presence of oxygen whilst cooling from 5000 K to 1000 K, including the formation of uranium oxides [31]. Work has also been completed regarding the oxidation of uranium, where a diffusion rate law was determined for the

oxidation of uranium at lower temperature (nonplasma) regimes [7, 32–34]. The plasma-forming experiments provide a different pathway to uranium product formation, condensing from much higher temperatures, whereas the experiments discussed in this document are more similar to that performed by Hertzberg et al., wherein a selection of metal powders were ignited to determine such characteristics as explosibility and burn velocity [35].

In this work, the dynamics, temperature, and gas phase environment of particulate combustion of natural uranium is characterized using absorption spectroscopy. Beneficially, absorption spectroscopy measurements can be used to quantitatively determine temperature and concentration of species with the knowledge of energy state information of targeted transitions [36, 37]. Few measurements are available on particulate combustion of U, which occurs after fragmentation from impact. Herein, high-speed imaging and

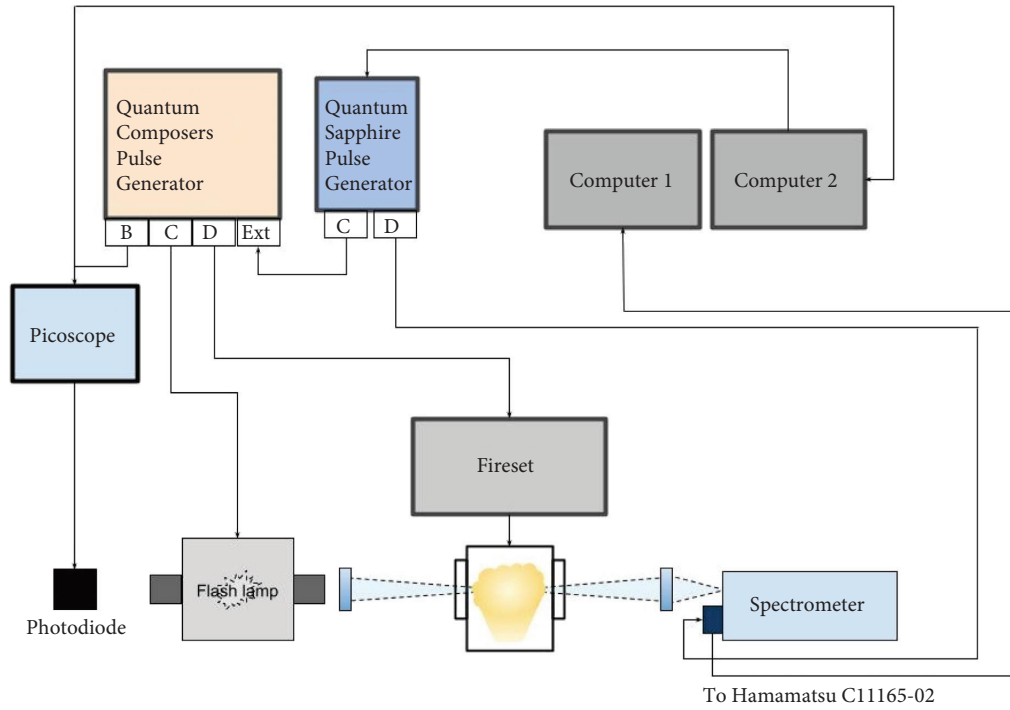


FIGURE 7: Entire dust cloud setup schematic for absorption measurements [38].

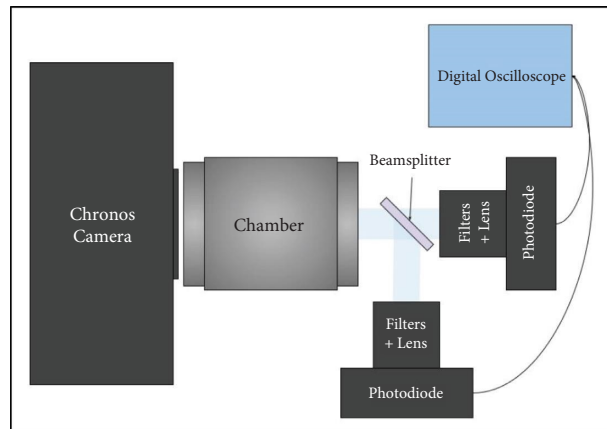


FIGURE 8: Top view schematic for metal powder burn time experiments [38].

TABLE 1: Powder characterization for burn time testing [15, 38, 48–59].

Element	Mass (mg)						Metal $\Delta H_{\text{vap},298\text{K}}^{\text{M}}$ (kJ/mol)	Oxide $\Delta H_{\text{vap},298\text{K}}^{\text{O}}$ (kJ/mol)	Oxide volatilization temperature (K)	Metal boiling point (K)	Source
U	6	3	2.6	4.1	3.6	5.4	477	621	~3800	4404	Reduced from oxide
Al	2.6	2.2	2.2	2.2	2.8	2.2	284	1860	4000	2791	Alfa aesar
B	2.4	3.5	2.3	2.3	2.3	—	499	360	2340	4139	Alfa aesar
Fe	3.3	2.3	3.5	3.2	3.2	2.6	354	610	3400	3133	Alfa aesar
Hf	3.9	2.8	2.4	—	—	—	648	1461	~4350	4575	Alfa aesar
Mo	3.8	3.6	3.7	3.4	3.6	—	617	333	900	5833	Alfa aesar
Si	2.6	2.3	2.7	—	—	—	383	353	2633	3177	Sigma aldrich
Ta	2.2	3.7	3.3	3.6	2.4	—	753	—	1200	5693	Alfa aesar
Ti	3	2.4	3	3.3	2.4	—	427	1890	3300	3631	Alfa aesar
W	2.3	2.3	3	3.8	3.1	—	774	452	1970	6203	Alfa aesar
Zr	2.2	3.9	3.7	—	—	—	591	920	4280	4703	Alfa aesar

TABLE 2: Information used to calculate Boltzmann temperature of Fe I from Kurucz database [38, 43].

λ (nm)	J_l	J_u	E_{lower} (cm^{-1})	A_{ul} (s^{-1})
381.584	4	3	11976.24	1.31E+08
382.0425	5	4	6928.268	6.67E+07
382.4444	4	3	0	2.83E+06
382.5881	4	3	7376.764	5.98E+07
382.7822	3	2	12560.93	1.05E+08
383.4222	3	2	7728.059	4.52E+07
384.0437	2	1	7985.784	4.70E+07
384.9966	1	0	8154.713	6.05E+07
385.6371	3	2	415.933	4.64E+06
385.9911	4	4	0	9.69E+06
386.5523	1	1	8154.713	1.55E+07
387.2501	2	2	7985.784	1.05E+07

broadband measurements of burn time provide additional insight into U combustion phenomena as well as that of other metal powders in order to establish comparisons between previously published data and observed uranium combustion behavior.

2. Materials and Methods

In order to ensure the validity of the uranium dust cloud combustion experiments described herein, the uranium powder was characterized using various methods prior to testing. Uranium powder was handled with precautions typically taken to avoid heavy metal inhalation and was on average $1.79 \mu\text{m}$ in particle diameter with a standard deviation of $2.58 \mu\text{m}$. A histogram of powder size distribution is shown in Figure 1. Powder sizes were derived from images acquired using a Field-Emission Environmental Scanning Electron Microscope (ESEM-FEG). Particle areas were found using ImageJ software, and diameters are reported as if from a circle of equivalent area since particles were irregularly shaped (Figure 2).

Images obtained were comparable to those shown in Ablitzer et al. in which uranium powders were imaged using SEM after being created from thermal dissociation of UH_3 powder [9]. For their work, these samples were in a hydrogen or inert argon environment aside from exposure to air during SEM sample preparation [9]. Qualitatively, their samples appear smoother than that shown in Figure 3, as samples for this study were stored in air. This is likely due to oxide formation on the surface of the particles exposed to air. Uranium is known to readily oxidize and form a protective refractory layer [8, 39, 40].

A scanning transmission electronic microscope (STEM) was used to characterize the oxide layer thickness of this uranium powder as well (Figure 4). The lighter “fuzzy” regions surrounding the particle are attributed to the uranium oxide layer, which is likely UO_2 or U_3O_8 (both are stable oxides). Smooth partially transparent uranium crystallites were observed in some images that were not included in this publication; however, the oxide layer exhibits a distinct texture. The oxide thickness was measured using ImageJ at regular intervals along the edges of many particles and a distribution was determined as shown in Figure 5. The

average oxide layer thickness was about 43.3 nm , with a standard deviation of 28.6 nm . The oxide layer can significantly affect particle combustion behavior and is discussed further later on.

A dust cloud chamber was created in order to facilitate the confined dispersal and combustion of $\sim 0.025 \text{ g}$ of uranium powder (Figure 6). Powder was loaded into a small conical cavity with two tungsten electrodes on opposite sides. The 5 kV discharge of a $1 \mu\text{F}$ capacitor generates a local plasma in the cavity that rapidly heats, ignites, and disperses the powder into the chamber above the cavity (see inset Figure 6). The internal volume of the chamber was $2.62E - 3 \text{ m}^3$. The chamber is capable of pressurization with a gas mixture of choice as well as vacuum down to a few torr (Figure 6).

Timing of the system was controlled with a pulse generator (Quantum Composers 9514) which delayed the acquisition of the event with respect to the firing of the dust cloud. An additional pulse generator (Quantum Sapphire 9214) was used to trigger line scan camera acquisition with a duration of $359.5 \mu\text{s}$ (Hamamatsu C11165-02). A digital oscilloscope (Picoscope 4424) and silicon photodiode were used for burn time measurement (Figure 7).

A Xenon flash lamp and custom-built 1.5 m spectrometer with 2400 gr/mm grating served as a broadband source to acquire an absorption spectrum of the gaseous combustion environment. The flash lamp has a duration of $7 \mu\text{s}$ full width at half maximum (FWHM) in this region. The system has a resolution of 0.0029 nm/pixel [42]. The spectral range targeted was between 381 and 387 nm due to an abundance of ground state U I and U II transitions [43]. Prior to the experiment, a reference spectrum of the flash lamp was taken and divided out from the spectrum acquired during the experiment, which would be taken at various delay times from the initial spark. The pathlength of the system was 5.08 cm . A Chronos 1.4 high-speed camera was also used to image uranium combustion at 4436.754 fps and $220.63 \mu\text{s}$ exposure. For the tests pertaining to this document, the ambient environment was air at atmospheric pressure.

Metal powder combustion has been studied extensively in the past, and burn time is a commonly used metric for its evaluation [44–47]. Burn time has strong dependence on particle size, temperature, and oxygen availability. Further

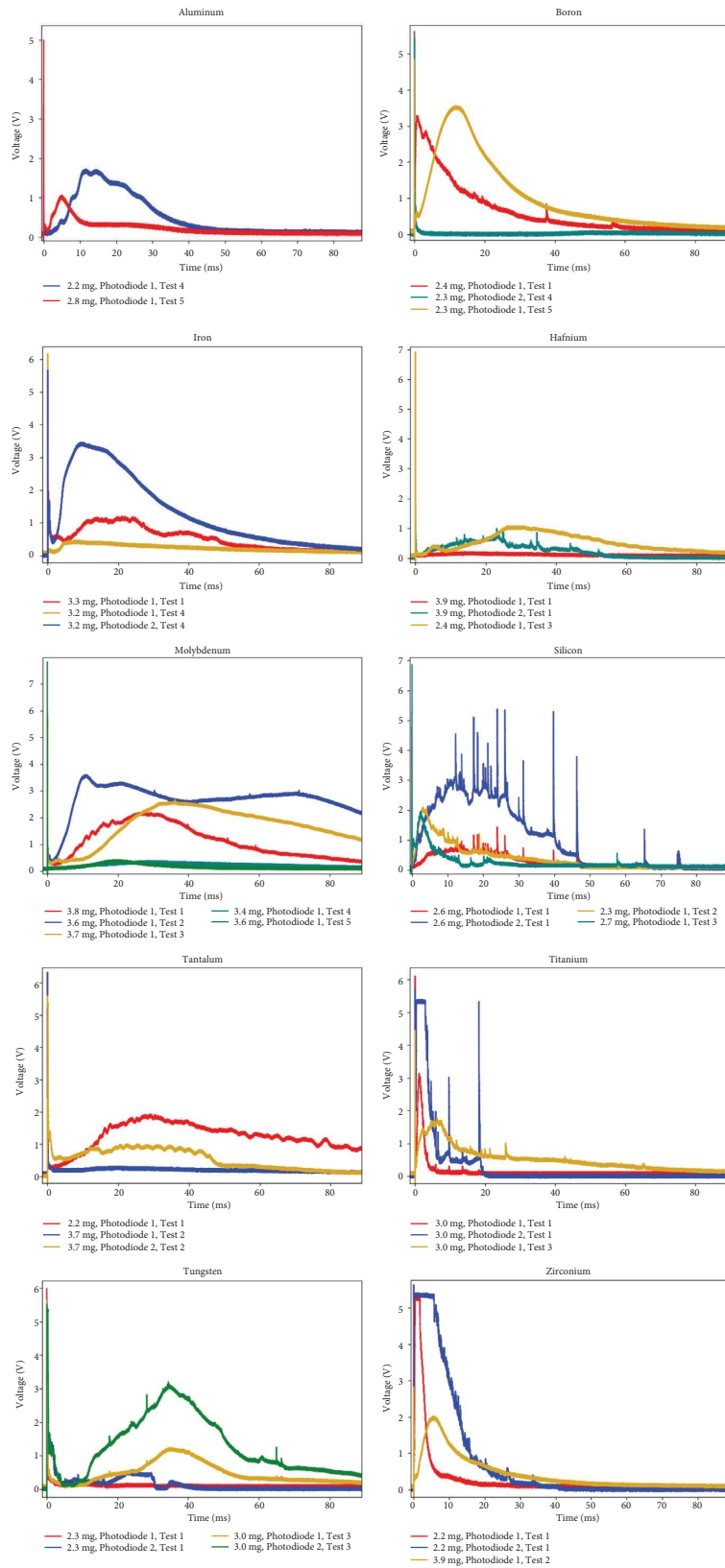


FIGURE 9: Selected photodiode traces used to determine burn times for various metals tested.

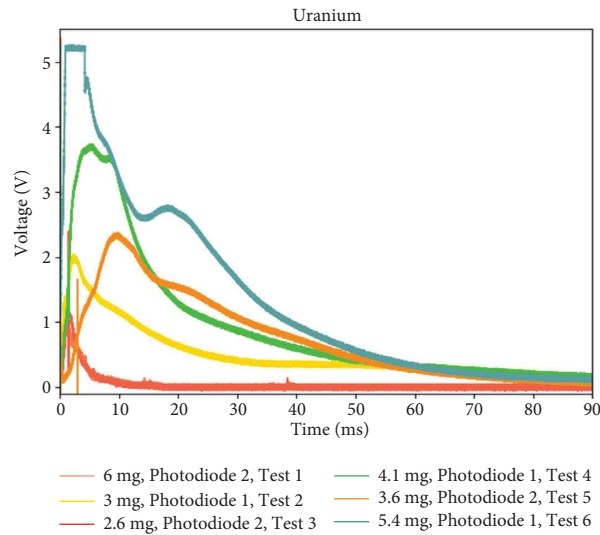


FIGURE 10: Photodiode intensity versus time.

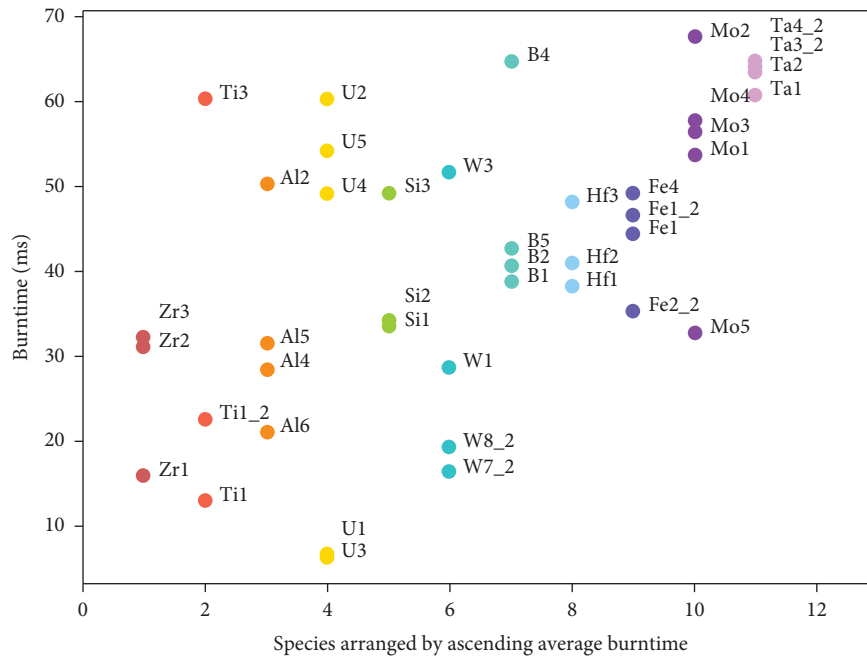


FIGURE 11: Burn time comparison between various metal powders.

tests to characterize burn times of various similarly sized ($<10\ \mu\text{m}$) metal powder (Ta, W, Zr, Hf, Al, B, Ti, Fe, Mo, and Si) dust clouds in air for comparison with uranium were conducted using a setup as shown in Figure 8.

Two photodiodes (Thorlabs PDA100A2) measured the intensity of broadband emissions from the combustion of $\sim 3\ \text{mg}$ of various metal powders as well as uranium. These photodiodes measured light from one of the chamber windows, which was split using a beamsplitter and attenuated using neutral density (ND) filtration to ensure that each test would have at least one signal without saturation. Uranium tests were also repeated for comparison and to confirm results from prior testing. Most of the powders were obtained commercially with $\geq 99\%$ purity from vendors summarized in

Table 1. The uranium powder was reduced from the oxide. Powders were then sieved using the Gilson Autosiever Sonic Sifter (GA-6) and 3-inch diameter $10\ \mu\text{m}$ sieve (GAA-83). Uranium powder was sifted by hand in a glovebox due to the high toxicity of inhalation. The Chronos 1.4 high speed color camera was used to image combustion as in previous uranium experiments, taking images every $300\ \mu\text{s}$.

These tests focused on both burn time acquisition and imaging to observe the occurrence of the exploding particle effect in an attempt to draw further conclusions about the nature of uranium particle combustion. Many of these powders and their burn characteristics have been studied in the past, and drawing commonalities between these and uranium can lead to a better understanding of the

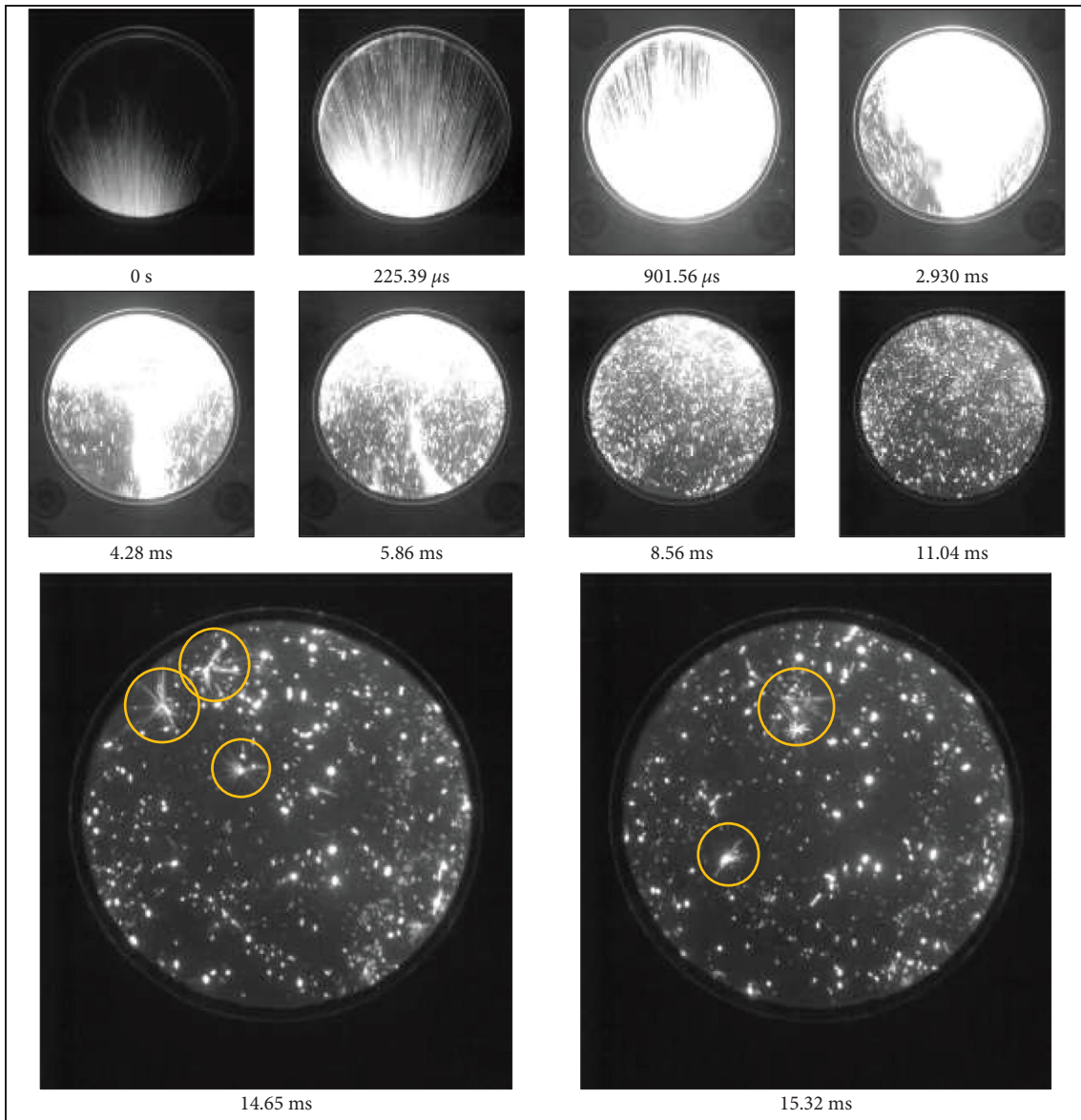


FIGURE 12: Storyboard of dust cloud combustion of 0.0287 g uranium in 1 atm air environment taken by Chronos 1.4 high speed monochrome camera at 4436.754 fps and 220.63 μs exposure. Circles indicate exploding agglomerates.

mechanisms through which uranium burns. Table 1 shows the data used to apply Glassman's criterion to data interpretation, where if the volatilization temperature of the oxide exceeds the boiling point of the metal, the metal shall combust in the vapor phase [58, 59]. Variation in mass used for each test is due to difficulty in measuring the minute quantities of powder necessary for these experiments. Charge masses were chosen to be within the expected flammability limits for the given chamber size, while providing reliable ignition using the existing experimental setup [41].

Since Fe transitions were prevalent in the spectra obtained from the uranium dust cloud. Table 2 shows the energy level information obtained from the Kurucz atomic spectral database used to calculate Boltzmann temperature for Fe I [43]. Iron has a lower temperature threshold for

vapor phase formation, and the signatures resulted from impurities present in the test chamber.

3. Results and Discussion

Burn time data was obtained for several metal powders that had been sifted to $<10\ \mu\text{m}$ in diameter and was quantified as the time between 10% and 90% of the area under the curves obtained from photodiode readouts (Figure 9). This methodology was chosen to eliminate the effect from the large initial spike seen in most of the data as well as to quantify when the bulk of the powder had been combusted. Repeatability is often an issue with metal combustion. Prior work indicates variability in combustion even in single particles of the same size, so repeated measurements should lead to a burn time distribution representative of a given

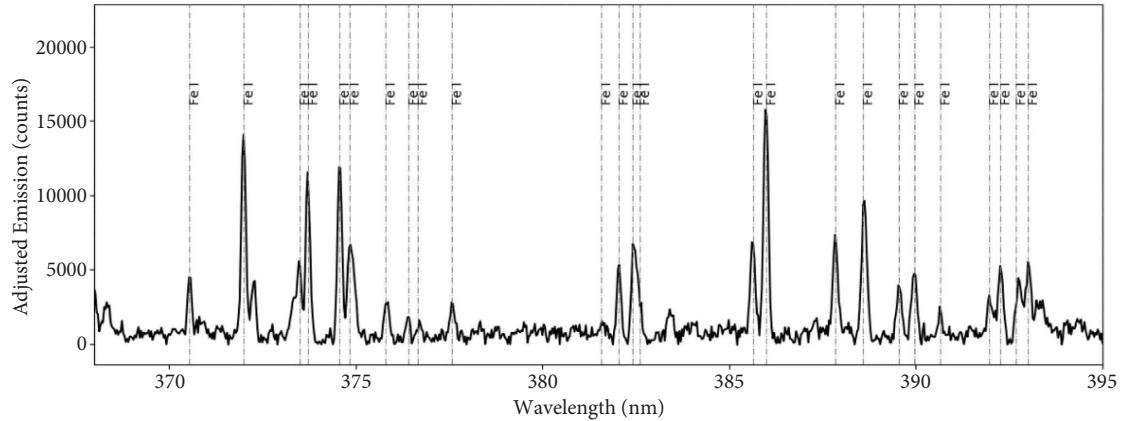


FIGURE 13: Emission from uranium dust cloud combustion in 1 atm air environment.

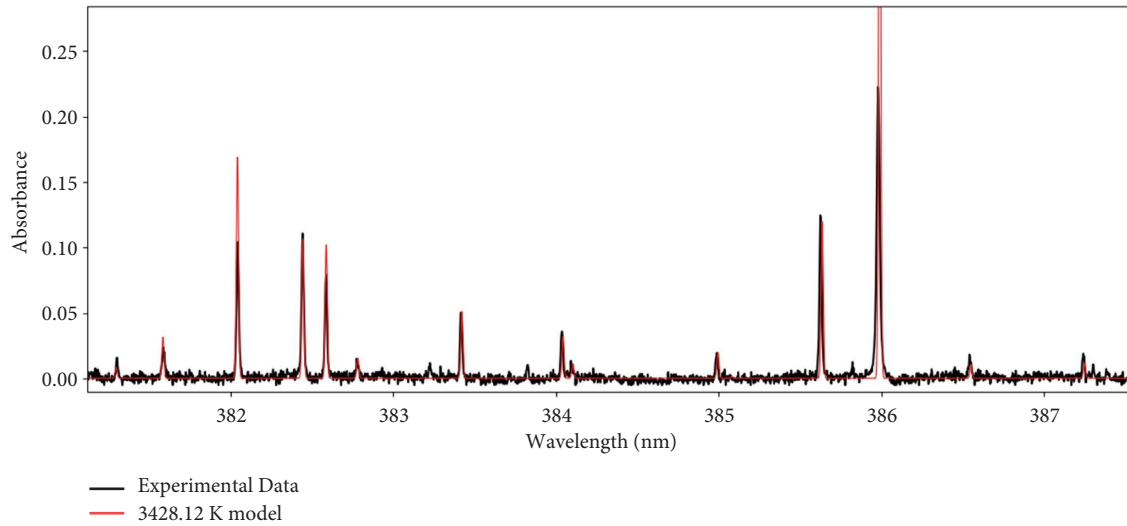


FIGURE 14: Absorbance at 1 ms delay from spark in 1 atm air. The red peaks are Fe I transitions modeled at the Boltzmann calculated temperature of 3428 K.

TABLE 3: Calculated adiabatic flame temperatures in air and O₂ at 1 atm and 300 K [10].

Element	Air (K)	O ₂ (K)
Al	3668.93	3968.53
B	4058.79	5543
Fe	3014.59	3383.55
Hf	4120 [35]	—
Mo	3191.98	4109.48
Si	3072.56	4899.67
Ta	3778.5	5062.85
Ti	3595.08	4461.72
W	3494.22	4374.91
Zr	4000.69	5118.31
U	3773.32	4843.2

material [60]. These experiments were designed to provide relative information on uranium combustion kinetics in the test configuration. All tests were performed in 1 atm air. Burning time data based on luminosity traces for Al, B, Hf, Fe, Mo, Si, Ta, Ti, W, Zr, and U dust clouds were obtained. It

is important to note that burning powders cannot necessarily be distinguished from other hot particles (i.e., oxide products) that may be present in the observed window, and that higher temperatures will dominate emission. Due to this, the calculation of these burn times involves the

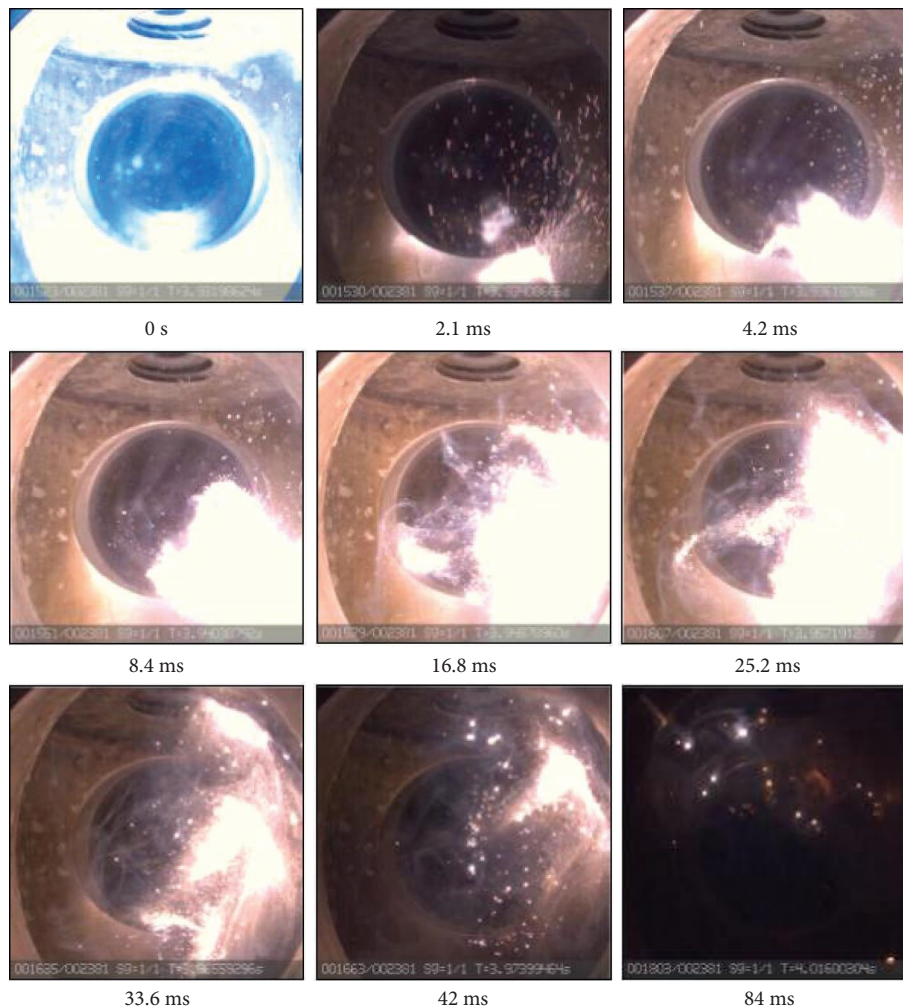


FIGURE 15: Aluminum dust cloud storyboard (2.2 mg).

assumption that all light emitted is due to burning and not other emissions. The Al burn times were comparable to those reported by Gill et al. for similar diameters [60]. B particle burn times were slightly longer than those previously reported for single-particle measurements in acetylene flames, but were similar to those from laser ignition [61]. Fe burn time was also comparable [62]. Titanium burn times were similar to those reported by Badiola and Dreizin for laser spark ignition, and Zr burn times were slightly longer [47]. Similar data for Hf, Mo, Si, Ta, and W were not found in the literature for particles of similar size.

There is some scatter in these measurements, possibly due to slight differences in masses tested or condensed phase emissions. Measurements in which photodiodes readings were saturated with light were excluded from this dataset since they would skew the calculation of burn time. The two photodiodes were measuring the same field of view with different amounts of neutral density (ND) filtration, so that if one saturated during a given test, time data might still be acquired by the other. Small particle explosions cause momentarily brighter emissions, causing spikes to appear in some of the data traces. This phenomenon is discussed later. Photodiode readings may also vary depending on locations

of particles, as although the field of view was maximized, parts of the chamber were obscured from view of the photodiodes. There is much particle movement from the initial upward jetting, impacts with the chamber surfaces, and subsequent falling and mixing.

As for uranium, some preliminary measurements can be found in Read's thesis [41]. Those burn times were much shorter than those reported in this document on average, possibly due to the much lower ambient pressures, different neutral density filtration (to prevent detector saturation) and larger masses tested (Figure 10).

Multiple of these materials were found to burn heterogeneously in the literature. Based on the previous work using this system, it is unlikely that temperatures over 4000 K were reached [41]. Burn times for each material tested are summarized in Figure 11. For some species, there is considerable variation in measurements.

These results on average correlate to relative burn time data in which Zr had shorter burn times than Ti for particles of roughly the same size [47] and results in which Al had longer burn times than Ti powders [63]. In tests of small amounts of high explosive materials doped with Al and B, B exhibited the slower burn rate [64]. Since these

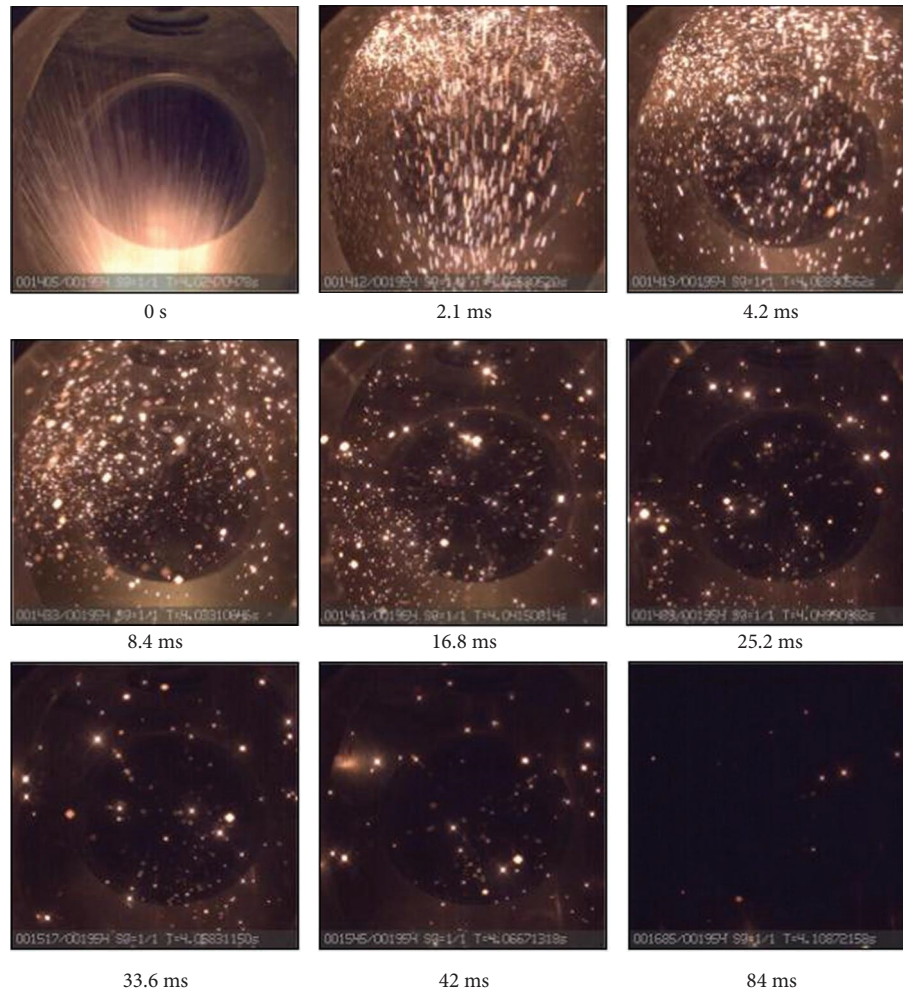


FIGURE 16: Boron dust cloud storyboard (2.4 mg).

data correlate with relative burn times found in other publications, it may be reasonable to conclude that U burn times are on average longer than that of Zr, Ti, and Al, and shorter than that of other species tested for particles of the same size.

Burn behavior was also observed for each material tested. At the temperature range tested, uranium is expected to burn heterogeneously, since its oxide volatilization temperature is lower than the metal boiling point. A storyboard of uranium dust cloud combustion is shown in Figure 12 in a 1 atm air environment.

Additionally, there is an exploding particle agglomerate effect at later times. This phenomenon is similar to that seen by Zepper et al. in aluminum combustion and by Dreizin in refractory materials such as zirconium and titanium [65–69]. As zirconium combusts in the presence of air, liquid ZrO_zN_y intermediates form and ZrO_2 precipitates out with gaseous nitrogen contained in voids. Newly exposed Zr burns with gaseous oxygen as the previously contained nitrogen escapes [66, 69]. A similar process occurs in titanium combustion, wherein a liquid solution of Ti, O, and N containing gaseous nitrogen contain voids simultaneously forms stable titanium oxides and an unreacted Ti surface

whilst gaseous nitrogen escapes [70]. It stands to reason that this sequence of events could also be occurring in the exploding particles of uranium based on the reported U-O and U-N phase diagrams [14, 15, 71, 72].

An appendix is provided with images from the combustion of other metal powders. Rather interestingly, powders that produced more robust clouds tended to have higher ignition temperatures in dust cloud environments as reported in the literature [73], but all ignition temperatures were still much lower than those reached by the system. W, Fe, and Mo were considered weakly explosible in comparison to other materials tested as determined by rate of pressure rise after ignition of the powder dust clouds, whereas Al, U, Ti, and Zr were considered severe [35, 73].

Spectral measurements were taken from uranium combustion to determine what emission or absorption features would appear in these conditions of excitation. Emission from a uranium dust explosion in a 1 atm air environment is shown in Figure 13. Continuum emission was subtracted out.

Fe I signatures from trace amounts of particulate present dominate the spectrum, indicating that the temperature of

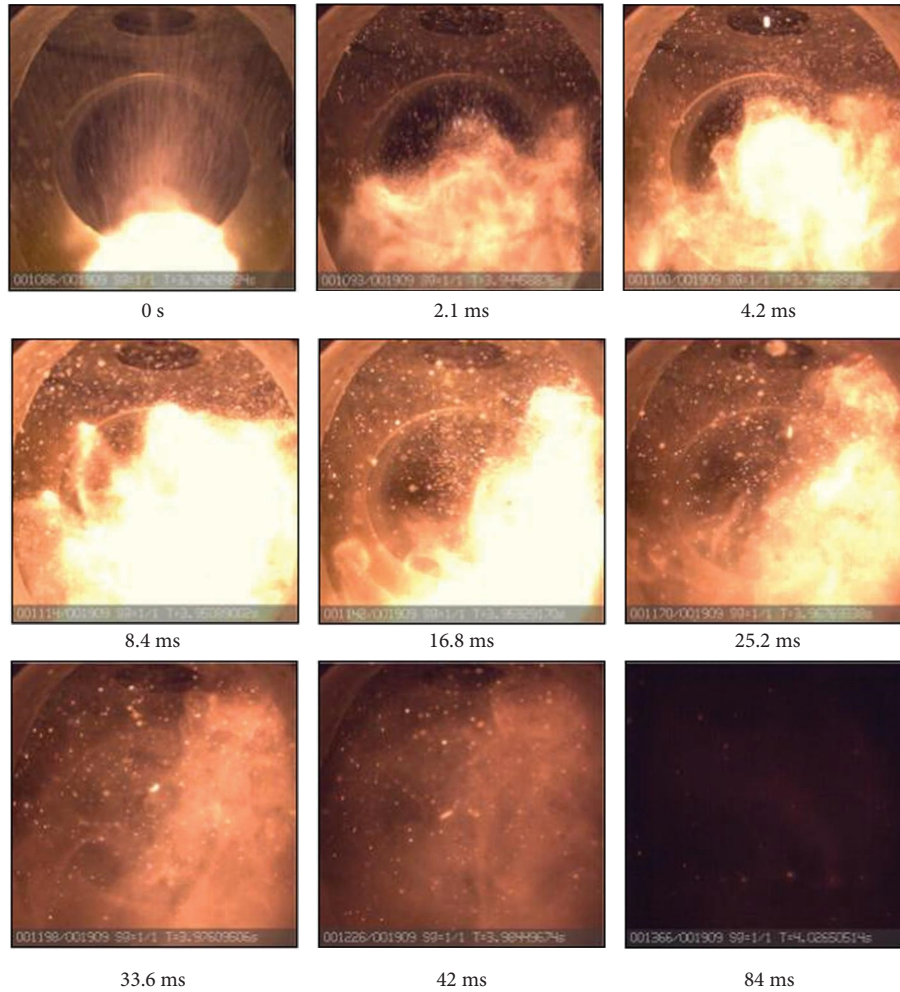


FIGURE 17: Fe dust cloud storyboard (3.3 mg).

combustion is insufficient to excite uranium transitions. Figure 14 shows the absorbance spectrum from combustion of uranium at a 1 ms delay from initial combustion with an overlaid model at a Boltzmann method calculated temperature of 3428 K. Assuming complete dispersal of the powder, the maximum concentration of uranium in the chamber should be 9.53 g/m^3 or $2.41E+22 \text{ atoms/m}^3$.

The concentration of iron in the chamber should be much lower than that of the uranium present, but iron transitions are excited at much lower temperatures than that of uranium. The iron concentration along the path measured was determined to be $1.967E+17 \text{ atoms/m}^3$ which corresponds to about $18.24 \mu\text{g}$. The total amount of uranium powder used in this test was 25 mg. Using the Beer-Lambert Law, and with the assumption of constant attenuation coefficient at a given moment along the optical path through the dust cloud, the detection limit of uranium was $2.781E+16 \text{ atoms/m}^3$ along the path from correlation to the ground state Fe I transition at 385.9911 nm. This region of the electromagnetic spectrum, $\sim 370\text{--}395 \text{ nm}$, has an abundance of ground state U I and U II transitions, which are highly likely to appear in absorption if vapor phase uranium is detected. This further corroborates the

conclusion that uranium is not burning in the vapor phase at this temperature.

Table 3 shows the adiabatic flame temperatures as calculated in NASA CEA in Air and O_2 for all powders tested with the exception of Hf, which was found in a Snyder [10, 35].

Of these elements, Fe had the lowest adiabatic flame temperature in Air, which corroborates its appearance in the vapor phase. Since vapor phase uranium signatures were not detected, it is likely that temperature in the system did not exceed $\sim 3773 \text{ K}$, which is supported by temperatures gleaned from emission and absorption measurements of the uranium dust cloud, consistently lower than that in Figure 14. The amount of uranium and oxygen present in the system would constitute a fuel lean mixture, and thus would burn at a lower maximum temperature, certainly lower than the volatilization temperature of uranium oxide and the boiling point of uranium. Badiola and Dreizin noted that NASA CEA code does not take into account nitride formation [47]. The observed temperature is somewhat higher than that theorized by Mouradian and Baker for uranium and zirconium spheres of this size regime burning in air [3].

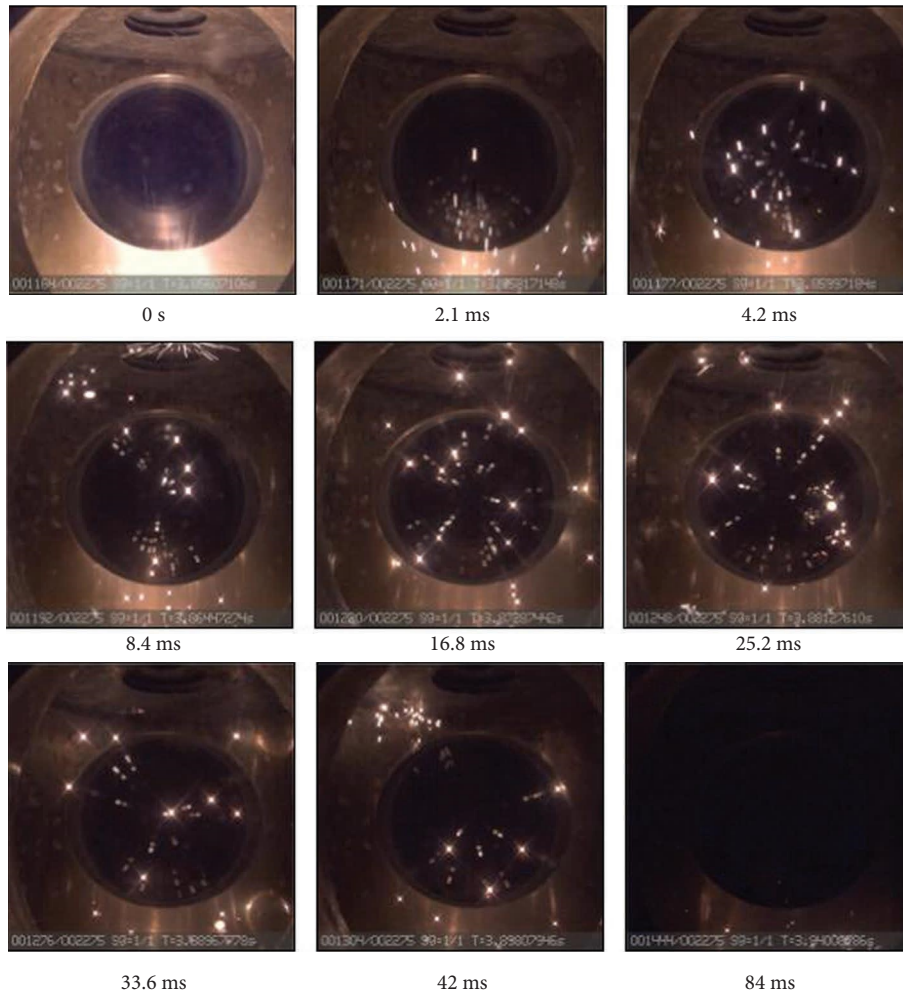


FIGURE 18: Hafnium dust cloud storyboard (3.9 mg).

Not much information was found dealing primarily with the burning of uranium aside from the prediction of burn temperatures and rates for uranium of various sizes and geometries [3], but similarities can be drawn from work on Zr. Like uranium, Zr behaves refractorily, burns heterogeneously, and exhibits the exploding particle effect described earlier. Combustion of micron regime Zr and Ti yields spectra reminiscent of blackbodies with no unique

discernible atomic transitions (aside from the iron impurity). Similarly, uranium transitions are absent from Figures 13 and 14. Uranium has a relatively thick protective oxide layer that further prevents the particle from entering the vapor phase, and it oxidizes readily [5, 39, 40, 74]. This oxide layer builds quickly, and that increased oxide layer thickness leads to increased emissivity [75].

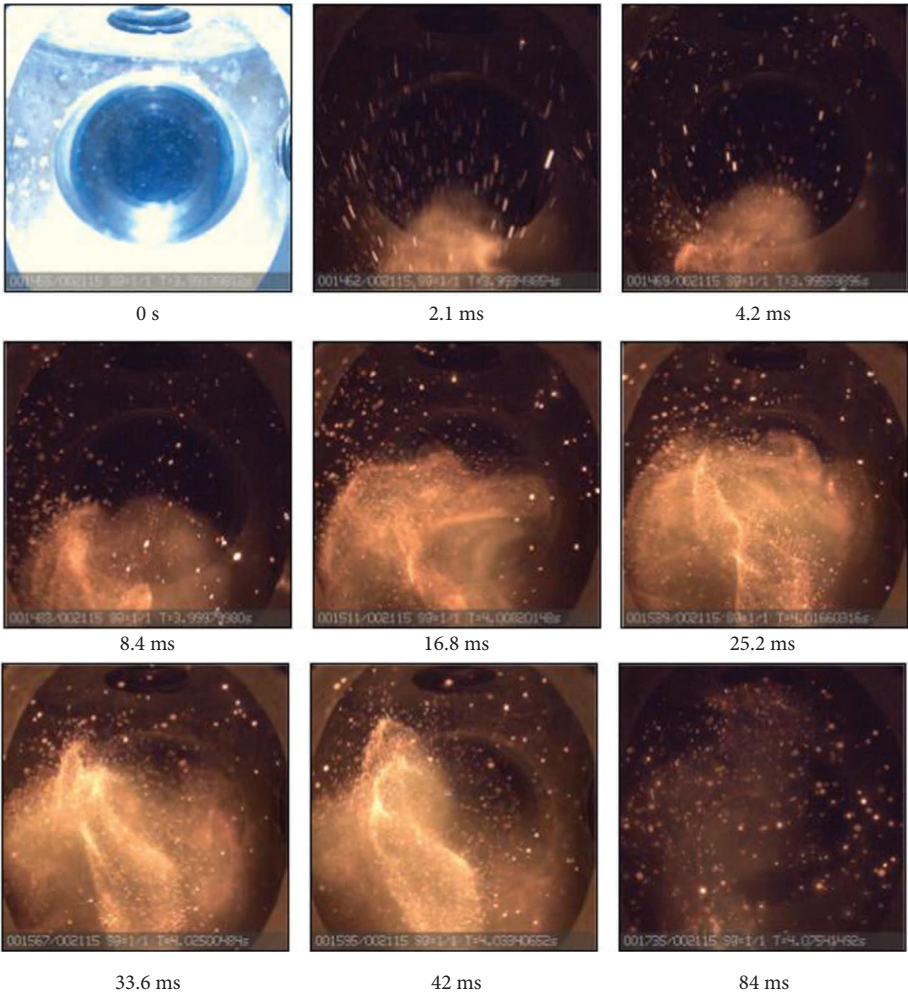


FIGURE 19: Molybdenum dust cloud storyboard (3.4 mg).

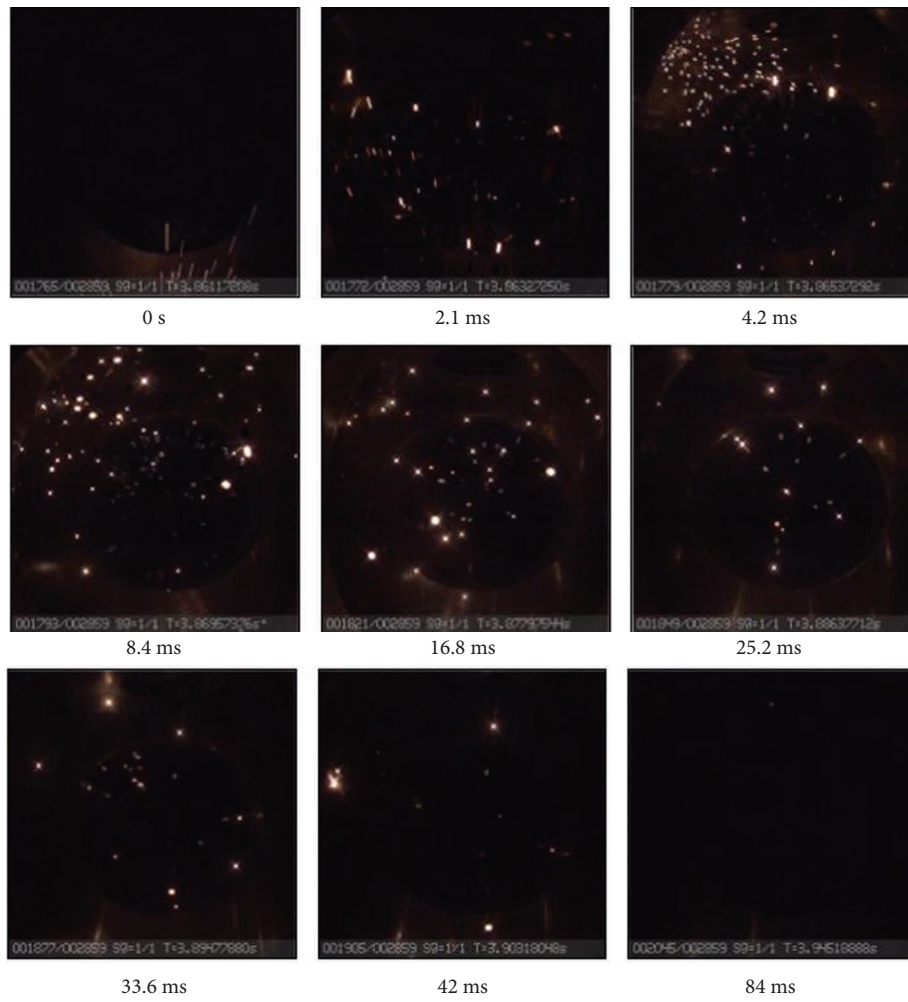


FIGURE 20: Silicon dust cloud storyboard (2.6 mg).

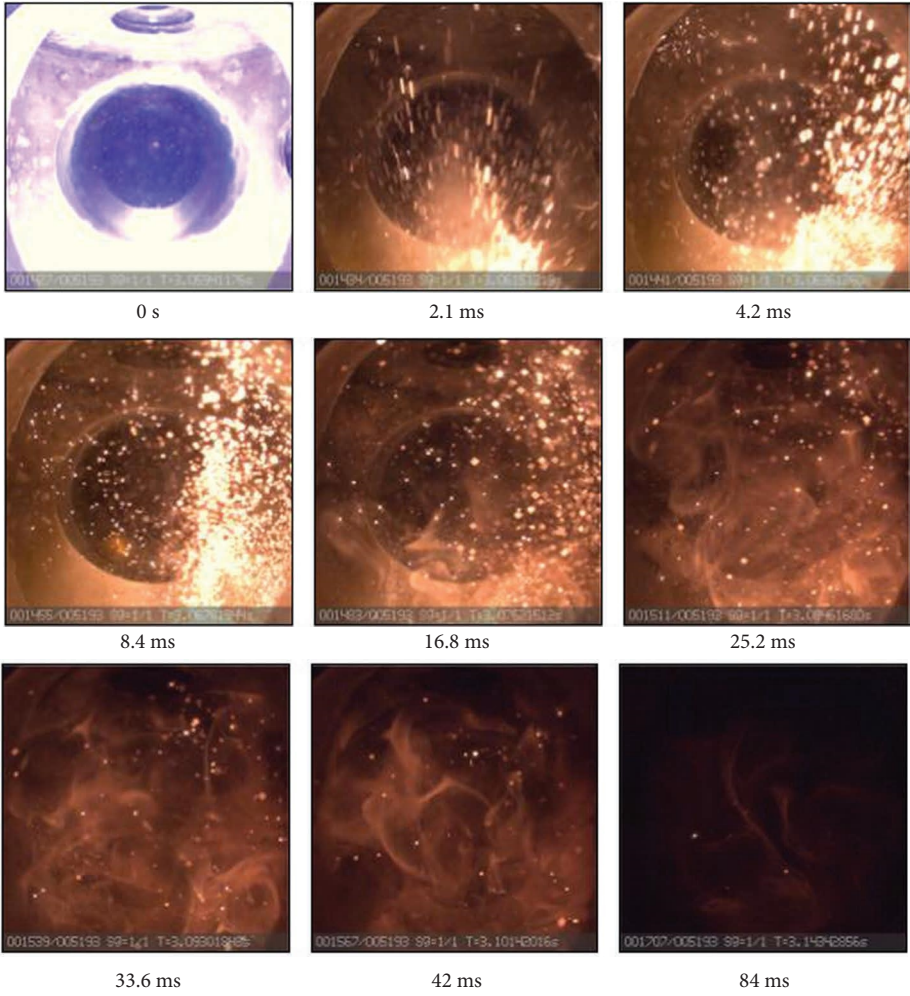


FIGURE 21: Tantalum dust cloud storyboard (shot 2, 2.8 mg).

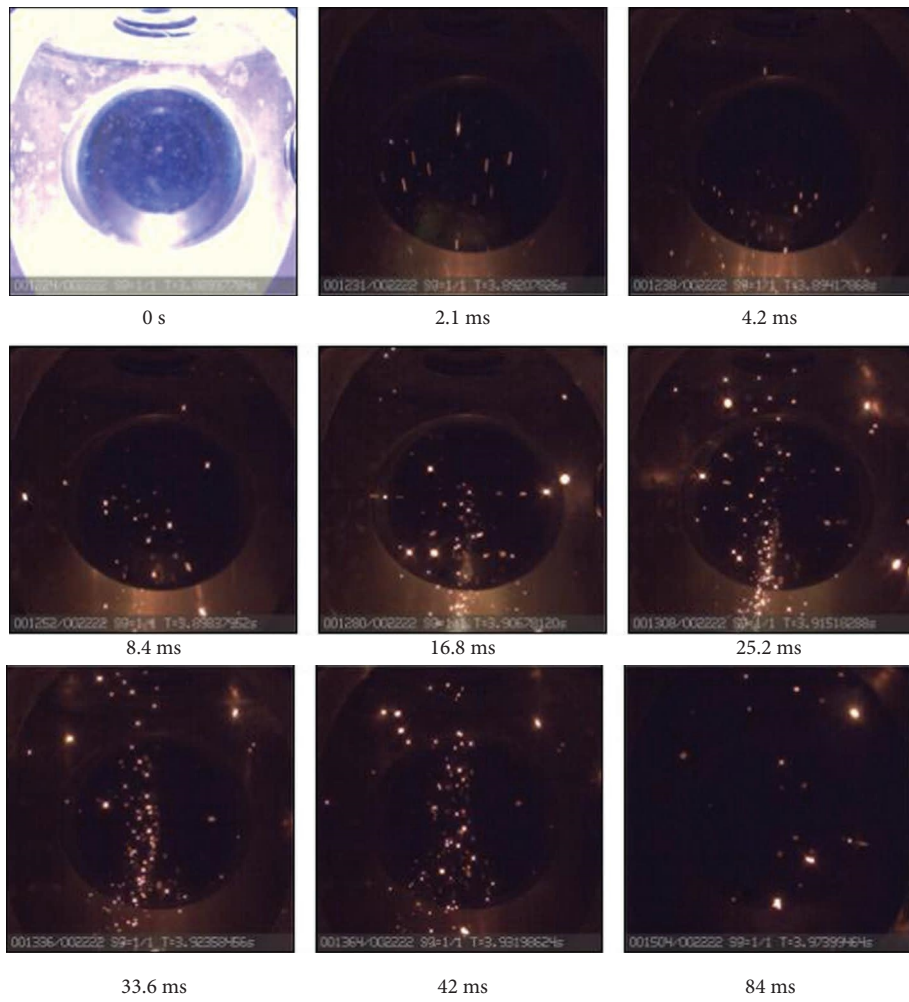


FIGURE 22: Tantalum dust cloud storyboard 2 (shot 1, 2.2 mg).

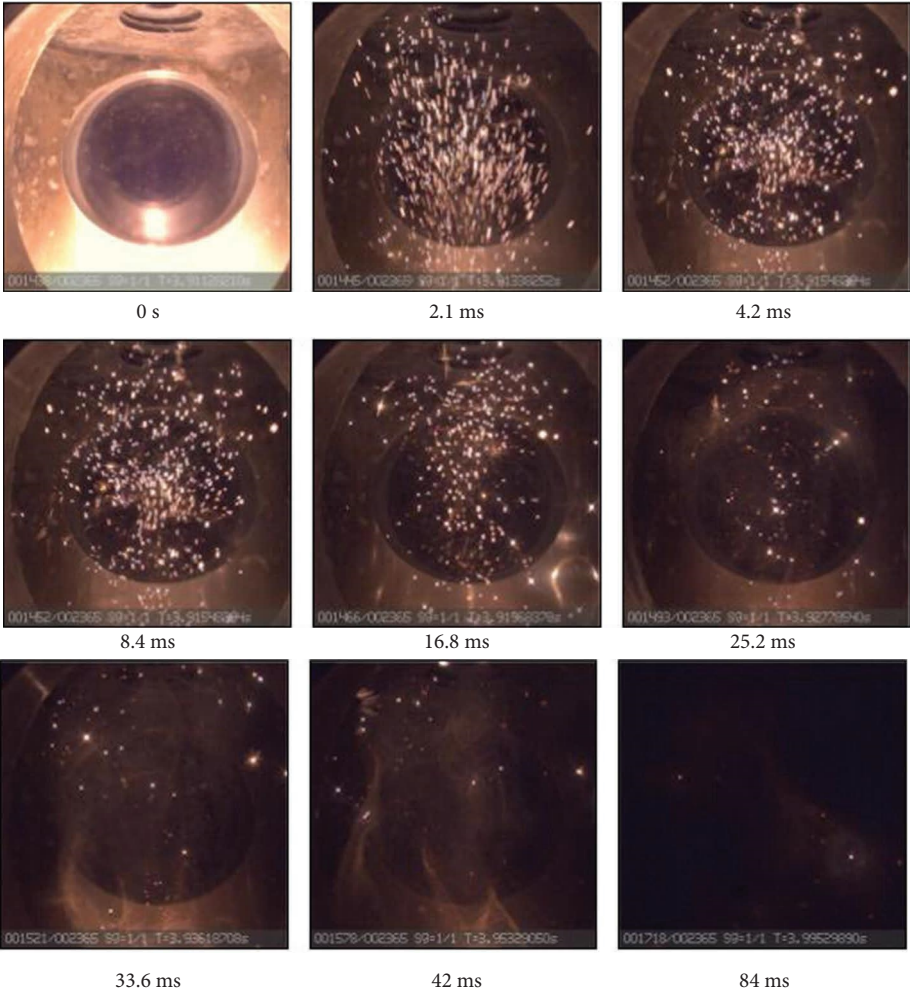


FIGURE 23: Titanium dust cloud storyboard (3.0 mg).

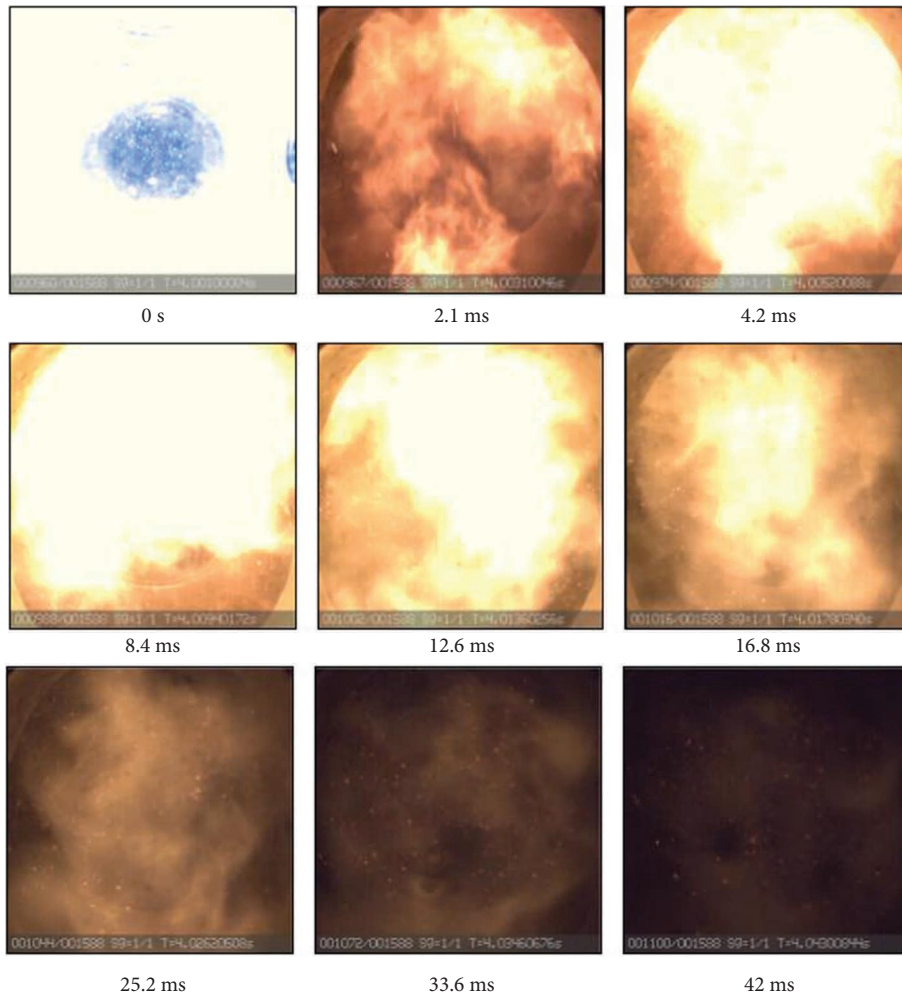


FIGURE 24: Tungsten dust cloud storyboard (3.0 mg).

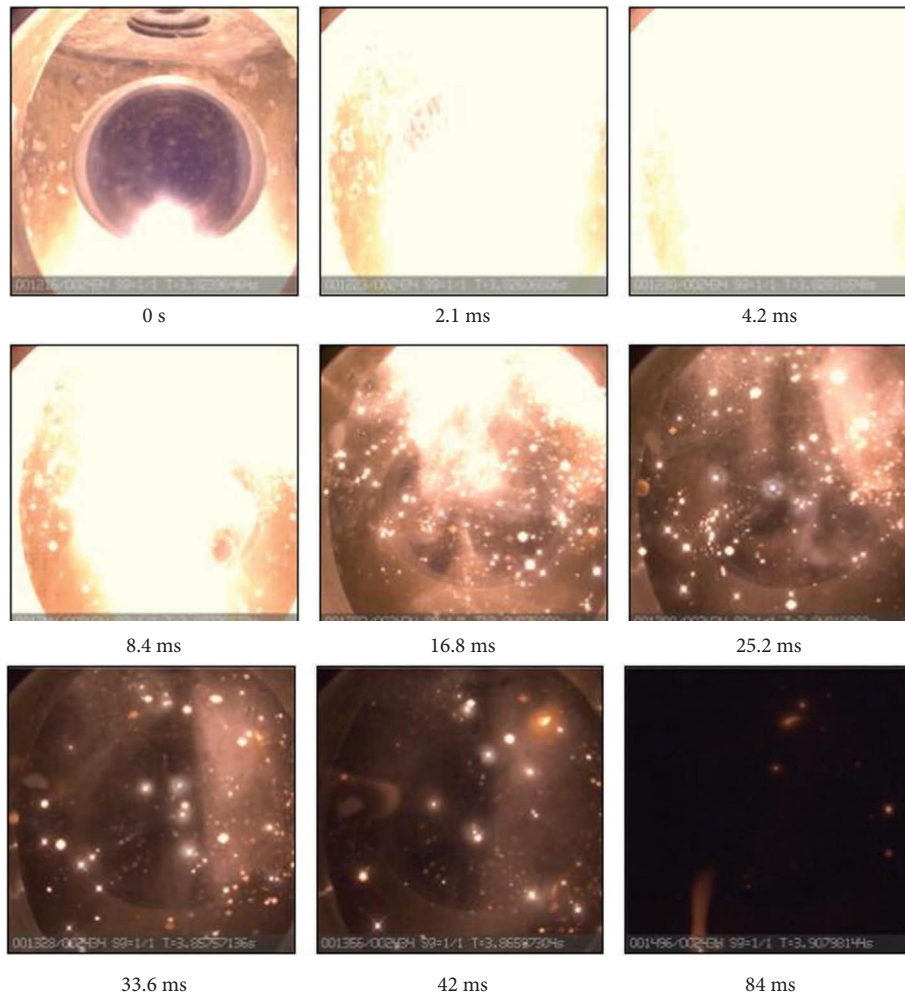


FIGURE 25: Zirconium dust cloud storyboard (3.7 mg).

4. Conclusions

From comparison to other metal powders, inferences were made about the dust cloud combustion of micron-sized uranium powder. It was determined that the burn temperature was limited to the volatilization temperature of uranium dioxide per Glassman's criterion, and that combustion behavior was similar to that of zirconium and other refractory metals in terms of burn time and exploding particle phenomena. From these similarities, it is conjectured that uranium also goes through the sequence of phase transitions, oxide precipitation, and gaseous nitrogen void formation during combustion that leads to this occurrence. Calculation of a detection limit from the Fe I signatures observed led to the conclusion that less than $\sim 2.781E + 16$ atoms/m³ U I was present in the path measured. This is due to the low temperatures achieved in the system (~ 3400 K) as compared to uranium oxide volatilization, as well as the strong containment of the uranium metal by the oxide, which inhibits vapor formation. Burn times yielded in this study seem consistent with relative burn times for different species from other publications; however, it may be beneficial to conduct a study on burn times of singular uranium particles to obtain a more accurate burn time. Similar work could be

performed under conditions of varying pressure and O₂ content, as well as shock tube heating of uranium powder at controlled temperature to observe change in spectra produced.

Appendix

Additional dust cloud storyboard images. (see Figures 15–25).

Data Availability

Data can be made available upon request from Nick Glumac: glumac@illinois.edu.

Conflicts of Interest

The authors declare that there are no conflicts of interest regarding the publication of this paper.

Acknowledgments

The authors are grateful to Ed Dreizin for his helpful discussion and suggestions. The authors would also like to

thank Catherine Wallace at the Beckman Institute at the University of Illinois at Urbana-Champaign for her expertise in acquisition of high-quality ESEM and STEM images. This work was supported by the Laboratory Directed Research and Development program at Sandia National Laboratories, a multimission laboratory managed and operated by National Technology and Engineering Solutions of Sandia LLC, a wholly owned subsidiary of Honeywell International Inc. for the U.S. Department of Energy's National Nuclear Security Administration under contract DE-NA0003525. This work was performed under the auspices of the U.S. Department of Energy by Lawrence Livermore National Laboratory under contract DE-AC52-07NA27344.

References

- [1] A. Bleise, P. R. Danesi, and W. Burkart, "Properties, use and health effects of depleted uranium (DU): a general overview," *Journal of Environmental Radioactivity*, vol. 64, no. 2-3, pp. 93-112, 2003.
- [2] E. J. Huber, C. E. Holley, and E. H. Meierkord, "The heats of combustion of thorium and Uranium_{1,2,3}," *Journal of the American Chemical Society*, vol. 74, no. 13, pp. 3406-3408, 1952.
- [3] E. M. Mouradian and L. Baker Jr., "Burning temperatures of uranium and zirconium in air," *Nuclear Science and Engineering*, vol. 15, no. 4, pp. 388-394, 1963.
- [4] F. Le Guyadec, X. Génin, J. P. Bayle, O. Dugne, A. Duhart-Barone, and C. Ablitzer, "Pyrophoric behaviour of uranium hydride and uranium powders," *Journal of Nuclear Materials*, vol. 396, no. 2-3, pp. 294-302, 2010.
- [5] L. Baker, J. G. Schnizlein, and J. D. Bingle, "The ignition of uranium," *Journal of Nuclear Materials*, vol. 20, no. 1, pp. 22-38, 1966.
- [6] R. F. Carter and K. Stewart, "On the oxide fume formed by the combustion of plutonium and uranium," *Inhaled Particles III*, vol. 2, 1970.
- [7] D. Cubicciotti, "The reaction between uranium and oxygen," *Journal of the American Chemical Society*, vol. 74, no. 4, pp. 1079-1081, 1952.
- [8] L. Baker and J. D. Bingle, "The kinetics of oxidation of uranium between 300 and 625°C," *Journal of Nuclear Materials*, vol. 20, no. 1, pp. 11-21, 1966.
- [9] C. Ablitzer, F. Le Guyadec, J. Raynal, X. Génin, and A. Duhart-Barone, "Influence of superficial oxidation on the pyrophoric behaviour of uranium hydride and uranium powders in air," *Journal of Nuclear Materials*, vol. 432, no. 1-3, pp. 135-145, 2013.
- [10] C. Snyder, *CEARUN*, NASA Glenn Research Center, Cleveland, OH, USA, 2019.
- [11] M. Bober and J. Singer, "Vapor pressure determination of liquid UO₂ using a boiling point technique," *Nuclear Science and Engineering*, vol. 97, no. 4, pp. 344-352, 2017.
- [12] C. Guéneau, M. Baichi, D. Labroche, C. Chatillon, and B. Sundman, "Thermodynamic assessment of the uranium-oxygen system," *Journal of Nuclear Materials*, vol. 304, no. 2-3, pp. 161-175, 2002.
- [13] G. H. Markstein, "Heterogenous reaction processes in metal combustion," *Symposium International on Combustion*, vol. 11, no. 1, 1967.
- [14] E. L. Dreizin, *Personal Communication*, 2021.
- [15] H. Okamoto, "O-U (Oxygen-Uranium)," *Journal of Phase Equilibria and Diffusion*, vol. 28, no. 5, p. 497, 2007.
- [16] P. R. Amyotte, M. P. Clouthier, and F. I. Khan, "Dust explosions: an overview," *Methods in Chemical Process Safety*, vol. 3, pp. 1-5, 2019.
- [17] R. A. Ogle, *Dust Explosion Dynamics*, Elsevier, Oxford, UK, 2017.
- [18] L. Türker, "Thermobaric and enhanced blast explosives (TBX and EBX)," *Defence Technology*, vol. 12, no. 6, pp. 423-445, 2016.
- [19] J. E. Geddie, *A Guide to Combustible Dusts*, Occupational Safety and Health Division, Raleigh, NC, USA, 2012.
- [20] C. Mitsakou, K. Eleftheriadis, C. Housiadis, and M. Lazaridis, "Modeling of the dispersion of depleted uranium aerosol," *Health Physics*, vol. 84, no. 4, pp. 538-44, 2003.
- [21] N. L. LaHaye and D. E. Burkes, *Metal Fuel Fabrication Safety and Hazards*, Pacific Northwest National Laboratory, Richland, WA, USA, 2019.
- [22] L. A. Kaledin, J. E. Mccord, and M. C. Heaven, "Laser spectroscopy of UO: characterization and assignment of states in the 0- to 3-ev range, with a comparison to the electronic structure of ThO," *Journal of Molecular Spectroscopy*, vol. 164, no. 1, pp. 27-65, 1994.
- [23] L. A. Kaledin and M. C. Heaven, "Electronic spectroscopy of UO," *Journal of Molecular Spectroscopy*, vol. 7, no. 185, p. 22, 1997.
- [24] S. S. Harilal, B. E. Brumfield, N. G. Glumac, and M. C. Phillips, "Elucidating uranium monoxide spectral features from a laser-produced plasma," *Optics Express*, vol. 26, no. 16, pp. 20319-20330, 2018.
- [25] P. J. Skrodzki, N. P. Shah, N. Taylor et al., "Significance of ambient conditions in uranium absorption and emission features of laser ablation plasmas," *Spectrochimica Acta Part B: Atomic Spectroscopy*, vol. 125, pp. 112-119, 2016.
- [26] K. C. Hartig, I. Ghebreziabher, and I. Jovanovic, "Standoff detection of uranium and its isotopes by femtosecond filament laser ablation molecular isotopic spectrometry," *Scientific Reports*, vol. 7, no. 1, pp. 1-9, 2017.
- [27] M. Miyabe, M. Oba, H. Iimura et al., "Absorption spectroscopy of uranium plasma for remote isotope analysis of next-generation nuclear fuel," *Applied Physics A*, vol. 112, no. 1, pp. 87-92, 2013.
- [28] X. K. Shen and Y. F. Lu, "Detection of uranium in solids by using laser-induced breakdown spectroscopy combined with laser-induced fluorescence," *Applied Optics*, vol. 47, no. 11, p. 1810, 2008.
- [29] R. Tyagi, Z. Zhang, and R. M. Pitzer, "Electronic spectrum of the UO and UO⁺ molecules," *The Journal of Physical Chemistry A*, vol. 118, no. 50, pp. 11758-11767, 2014.
- [30] M. S. Finko, D. Curreli, D. G. Weisz et al., "A model of early formation of uranium molecular oxides in laser-ablated plasmas," *Journal of Physics D: Applied Physics*, vol. 50, no. 48, Article ID 485201, 2017.
- [31] B. Koroglu, S. Wagnon, Z. Dai et al., "Gas phase chemical evolution of uranium, aluminum, and iron oxides," *Scientific Reports*, vol. 8, no. 1, pp. 1-15, 2018.
- [32] K. Hauffe, *Oxidation of Metals*, Plenum Press, New York, NY, USA, 1965.
- [33] P. J. Hayward, D. G. Evans, P. Taylor, I. M. George, and A. M. Duclos, "Oxidation of uranium in argon-25% oxygen at 190-610°C," *Journal of Nuclear Materials*, vol. 187, 1992.
- [34] L. G. Stonhill, "The determination of atomic ratios in the uranium-oxygen system by a thermogravimetric method," *Canadian Journal of Chemistry*, vol. 37, 1959.
- [35] M. Hertzberg, I. A. Zlochower, and K. L. Cashdollar, "Metal dust combustion: explosion limits, pressures, and

- temperatures," *Symposium (International) on Combustion*, vol. 24, no. 1, pp. 1827–1835, 1992.
- [36] R. K. Hanson, R. M. Spearrin, and C. S. Goldenstein, *Spectroscopy and Optical Diagnostics for Gases*, Springer, Berlin, Germany, 2016.
- [37] N. M. Laurendeau, *Statistical Thermodynamics, Fundamentals and Applications*, Cambridge University Press, Cambridge, UK, 2005.
- [38] E. N. Weerakkody, *Spectral Characterization of Actinide Signatures for Nuclear Remote Sensing Applications*, University of Illinois at Urbana-Champaign, Urbana, IL, USA, 2021.
- [39] E. G. Rauh and R. J. Thorn, "Vapor pressure of uranium," *The Journal of Chemical Physics*, vol. 22, no. 8, pp. 1414–1420, 1954.
- [40] T. C. Totemeier, *A Review of the Corrosion and Pyrophoricity Behavior of Uranium and Plutonium*, Argonne National Laboratory, Idaho Falls, ID, USA, 1995.
- [41] B. A. Read, *A Review of Optical Diagnostic Techniques Used to Identify Uranium Spectral Signatures*, Aerospace Engineering Department, University of Illinois at Urbana-Champaign, Urbana, IL, USA, 2018.
- [42] E. N. Weerakkody and N. G. Glumac, "Quantitative absorption spectroscopy of laser-produced plasmas," *Journal of Physics D: Applied Physics*, vol. 54, no. 12, Article ID 125201, 2021.
- [43] P. L. Smith, C. Heise, J. R. Esmen, and R. L. Kurucz, *Division of Plasmaphysics—Atomic Spectral Line Database*, Hannover University, Hanover, Germany, 2018.
- [44] M. J. Spalding, *Boron Particle Ignition and Combustion in a Shock Tube Using Time-Resolved Spectroscopy*, Mechanical Engineering Department, University of Illinois at Urbana-Champaign, Urbana, IL, USA, 2000.
- [45] E. L. Dreizin, A. V. Suslov, and M. A. Trunov, "General trends in metal particles heterogeneous combustion," *Combustion Science and Technology*, vol. 90, no. 1–4, pp. 79–99, 1993.
- [46] J. Guadarrama, *Burn Time Measurements of Micron Sized Al-Mg Alloys and Mg in a Heterogeneous Shock Tube in Different Oxidizing Environments*, Mechanical Science and Engineering, University of Illinois at Urbana-Champaign, Urbana, IL, USA, 2016.
- [47] C. Badiola and E. L. Dreizin, "Combustion of micron-sized particles of titanium and zirconium," *Proceedings of the Combustion Institute*, vol. 34, no. 2, pp. 2237–2243, 2013.
- [48] Y. Zhang, J. R. G. Evans, and S. Yang, "Corrected values for boiling points and enthalpies of vaporization of elements in handbooks," *Journal of Chemical & Engineering Data*, vol. 56, no. 2, pp. 328–337, 2011.
- [49] R. W. Ohse, "High-temperature vapor-pressure studies of UO_2 by the effusion method and its thermodynamic interpretation," *The Journal of Chemical Physics*, vol. 44, no. 4, pp. 1375–1378, 1966.
- [50] J. W. McMurray, "Characterization of urania vaporization with transpiration coupled thermogravimetry," *Journal of Chemical Thermodynamics*, vol. 95, 2015.
- [51] M. B. Panish and L. Reif, "Thermodynamics of the vaporization of Hf and HfO_2 : dissociation energy of HfO ," *The Journal of Chemical Physics*, vol. 38, no. 1, pp. 253–256, 1963.
- [52] H. Okamoto, "Hf-O (Hafnium-Oxygen)," *Journal of Phase Equilibria and Diffusion*, vol. 29, no. 1, p. 124, 2008.
- [53] S. J. Schneider, *Compilation of the Melting Points of the Metal Oxides*, U. S. Department of Commerce, Washington, DC, USA, 1963.
- [54] G. L. Humphrey, "Heats of formation of Tantalum, niobium and zirconium oxides, and Tantalum carbide," *Journal of the American Chemical Society*, vol. 76, no. 4, pp. 978–980, 1954.
- [55] L. Brewer, "Thermodynamic properties of the oxides and their vaporization processes," *Chemical Reviews*, vol. 52, no. 1, pp. 1–75, 1953.
- [56] Q. N. Nguyen, *High Temperature Volatility and Oxidation Measurements of Titanium and Silicon Containing Ceramic Materials*, Cleveland State University, Cleveland, OH, USA, 2008.
- [57] B. P. E. Blackburn, M. Hoch, and H. L. Johnston, "The vaporization of molybdenum and tungsten oxides," *Journal of Physical Chemistry*, vol. 62, no. 7, pp. 769–773, 1958.
- [58] I. Glassman, R. A. Yetter, and N. G. Glumac, *Combustion*, Elsevier, Amsterdam, Netherlands, 5th edition, 2015.
- [59] I. Glassman, *Metal Combustion Processes*, Princeton University, Princeton, New Jersey, 1959.
- [60] R. J. Gill, S. Mohan, and E. L. Dreizin, "Sizing and burn time measurements of micron-sized metal powders," *Review of Scientific Instruments*, vol. 80, no. 6, Article ID 064101, 2009.
- [61] K. A. Chintersingh, *Improving Boron for Combustion Applications*, New Jersey Institute of Technology, Newark, NJ, USA, 2019.
- [62] J. H. Sun, R. Dobashi, and T. Hirano, "Combustion behavior of iron particles suspended in air," *Combustion Science and Technology*, vol. 150, no. 1–6, pp. 99–114, 2000.
- [63] S. Wang, S. Mohan, and E. L. Dreizin, "Effect of flow conditions on burn rates of metal particles," *Combustion and Flame*, vol. 168, pp. 10–19, 2016.
- [64] A. Korotkikh, I. Sorokin, and E. Selikhova, "Ignition and combustion of high-energy materials containing aluminum, boron and aluminum diboride," *MATEC Web of Conferences*, vol. 194, Article ID 01055, 2018.
- [65] E. T. Zepper, M. L. Pantoya, S. Bhattacharya, J. O. Marston, A. A. Neuber, and R. J. Heaps, "Peering through the flames: imaging techniques for reacting aluminum powders," *Applied Optics*, vol. 56, no. 9, pp. 2535–2541, 2017.
- [66] E. L. Dreizin, "Effect of phase changes on metal-particle combustion processes," *Combustion, Explosion and Shock Waves*, vol. 39, no. 6, pp. 681–693, 2003.
- [67] P. Lipetzky, "Refractory metals: a primer," *Journal of Occupational Medicine*, vol. 54, no. 3, pp. 47–49, 2002.
- [68] E. C. Freiling, "Radionuclide fractionation in bomb debris," *Science*, vol. 133, no. 3469, pp. 1991–1998, 1961.
- [69] I. E. Molodetsky, E. L. Dreizin, and C. K. Law, "Evolution of particle temperature and internal composition for zirconium burning in air," *Symposium (International) on Combustion*, vol. 26, no. 2, pp. 1919–1927, 1996.
- [70] I. E. Molodetsky, E. P. Vicenzi, E. L. Dreizin, and C. K. Law, "Phases of titanium combustion in air," *Combustion and Flame*, vol. 112, no. 4, pp. 522–532, 1998.
- [71] T. Hiroaki, "Phase relations and thermodynamic properties of the uranium-nitrogen system," *Journal of Nuclear Materials*, vol. 51, no. 1, pp. 78–89, 1974.
- [72] P.-Y. Chevalier, E. Fischer, and B. Cheynet, "Progress in the thermodynamic modelling of the O-U binary system," *Journal of Nuclear Materials*, vol. 303, no. 1, pp. 1–28, May 2002.
- [73] M. Jacobson, A. R. Cooper, and J. Nagy, "Explosibility of metal powders," *Bureau of Mines Report of Investigations*, vol. 6516, p. 20, 1964.
- [74] V. G. Ioffe, "Inflammability of zirconium powders and its alloys in the suspended state," *Poroshkovaya Metallurgiya*, vol. 3, pp. 100–104, 1968.
- [75] C. W. Solbrig, *Heat Release Rate from the Combustion of Uranium*, Argonne National Lab, Idaho Falls, ID, USA, 1995.